Influence of Spherical Particle Size Distribution on Pressure Gradients in Mixed Bed

Jin Ho Park, Mooneon Lee, Eunho Kim, Hyun Sun Park*
Division of Advanced Nuclear Engineering, POSTECH, Pohang, Gyungbuk, Republic of Korea 37673
**Corresponding author: hejsunny@postech.ac.kr*

1. Introduction

When severe accidents occur in nuclear power plants, it is crucial to assure coolability of the relocated corium on the reactor containment floor because this situation causes concrete floor erosion due to molten corium concrete interaction (MCCI) without sufficient coolant injection into the debris bed. Therefore, it is of key importance to ensure the long-term cooling of the relocated corium on the reactor containment floor by supplying coolant into the debris bed for stabilization and termination of the severe accident progression. Since the cooling mechanism is governed by pressure gradients which depend on the debris bed characteristics such as particle morphology, size distribution and bed porosity etc., it is necessary to investigate the two-phase flow pressure gradient mechanism in the debris bed under the conditions of hypothetical severe accident cases. The debris bed characteristics in such accident conditions can be found from previous molten fuel-coolant interactions (FCIs) studies. In the FCIs experiments, the quenched particulate debris bed is composed of irregular shape particles with size distribution from a few of micro-meters to about 10 mm. [1] Thus, this study focused on the influence of particle size distribution on pressure gradients in mixed bed.

2. Models

To consider the influence of particle size distribution on pressure gradients of single-phase flow in porous media, various mean particle diameters (mass, d_m; area, d_a; length, d_l; and number, d_n) have been suggested as the effective diameter assuming that the Ergun equation is valid for mixed beds. [2] The Ergun equation, Eq. 1 is a momentum conservation equation for single-phase flow in porous media composed of single-size spherical particles.

$$-\frac{dp}{dz}-\rho_f g=\frac{\mu}{K}V_s+\frac{\rho_f}{\eta}V_s^2 \quad (1)$$

On the right-hand side of Eq. 1, the first term is viscous energy loss term and the second term is inertial energy loss term, μ [Pa·s] and ρ_f [kg/m^3] are the dynamic viscosity and the density of fluid, respectively; $-dp/dz$ [Pa/m] represents pressure loss in porous media which is composed of single size particles with the diameter of d_p [m]. V_s [m/s] is the superficial velocity of fluid and the bed porosity, Eq. 2 is calculated by the total mass of particles, $\sum m_p$ [kg] in the test section, the density of particles, ρ_p [kg/m^3] and the volume of the test section, V_t [m^3].

$$\varepsilon = 1 - \frac{\sum m_p / \rho_p}{V_t} \quad (2)$$

In the case of the permeability, Eq. 3, a measure of the flow conductance of the matrix, and the passability, Eq. 4, a quality of being passable, are calculated by

$$K=\frac{\varepsilon^3 d_p^{\,2}}{150(1-\varepsilon)^2} \quad (3)$$

$$\eta=\frac{\varepsilon^3 d_p}{1.75(1-\varepsilon)} \quad (4)$$

For two-phase flow through debris bed, various analytical models (Reed, Lipinski, Hu & Theofanous, Schulenberg & Müller, Tung & Dhir etc.) [3 – 6] have been suggested based on the Ergun equation by including the relative permeabilities and passabilities with/without the consideration of the interfacial friction between the liquid and the gas. They are expressed by Eq. 5 – 6 for the liquid and the gas, respectively.

$$-\frac{dp_l}{dz}=\rho_l g+\frac{\mu_l}{K\cdot K_{rl}}V_{sl}+\frac{\rho_l}{\eta\cdot\eta_{rl}}|V_{sl}|\cdot V_{sl}-\frac{F_i}{s} \quad (5)$$

$$-\frac{dp_g}{dz}=\rho_g g+\frac{\mu_g}{K\cdot K_{rg}}V_{sg}+\frac{\rho_g}{\eta\cdot\eta_{rg}}|V_{sg}|\cdot V_{sg}+\frac{F_i}{\alpha} \quad (6)$$

where K_{rl}, K_{rg} [m^2] and η_{rl}, η_{rg} [m] are the relative permeabilities and passabilities of the liquid and the gas, respectively; F_i is the interfacial friction; s is saturation ($=1-\alpha$); V_{sl} [m/s] and V_{sg} [m/s] are the superficial velocities of the liquid and the gas, respectively. The relative permeabilities and passabilities in the models without interfacial friction are listed in Table I.

Table I: Relative permeabilities and passabilities in the models without consideration of the interfacial friction

	K_{rg}	η_{rg}	K_{rl}	η_{rl}	F_i
Reed	α^3	α^5	s^3	s^5	-
Lipinski	α^3	α^3	s^3	s^3	-
Hu & Theofanous	α^3	α^6	s^3	s^6	-

Table II: Relative permeabilities, passabilities and the interfacial friction in Schulenberg & Müller model

	K_{rg}	η_{rg}	K_{rl}	η_{rl}
Schulenberg & Müller	α^3	$0.1\alpha^4$ $(\alpha \le 0.3)$ α^6 $(\alpha > 0.3)$	s^3	s^5

* $F_i : 350 s^7 \alpha \frac{\rho_l K}{\eta \sigma} (\rho_l - \rho_g) g (\frac{V_{sg}}{\alpha} - \frac{V_{sl}}{s})^2$

In the case of the models considering interfacial friction explicitly, the relative permeabilities, passabilities, and the interfacial frictions are listed in Table II – IV. As a result of visualization in water/air flow experiments, Tung & Dhir defined flow regimes according to void fraction, α. In table III, α_1 is defined by the minimum value between 0.3 and $0.6(1-\gamma)^2$ where γ is the ratio of the bubble diameter, D_b, Eq. 7 and the particle diameter, d_p; $\alpha_2 = \pi/6 \approx 0.52$, $\alpha_3 = 0.6$, $\alpha_4 = \pi\sqrt{2}/6 \approx 0.74$. The interfacial frictions and its coefficients according to the flow regime are listed in Table IV. In here, the relative velocity, V_r and the geometric factor, f are defined by Eq. 8 – 9, respectively. For smooth transition between flow regimes, the weighting function was defined and more specific information is in their paper. [6]

Table III: Relative permeabilities and passabilities according to flow regime in Tung & Dhir model

	Flow regime	K_{rg}	η_{rg}	K_{rl}	η_{rl}
α_1	Bubbly	$(\frac{1-\varepsilon}{1-\varepsilon\alpha})^{4/3}\alpha^4$	$(\frac{1-\varepsilon}{1-\varepsilon\alpha})^{2/3}\alpha^4$	s^4	s^4
α_2	Transition	-	-		
α_3	Slug	$(\frac{1-\varepsilon}{1-\varepsilon\alpha})^{4/3}\alpha^4$	$(\frac{1-\varepsilon}{1-\varepsilon\alpha})^{2/3}\alpha^4$		
α_4	Transition	-	-		
	Annular	$(\frac{1-\varepsilon}{1-\varepsilon\alpha})^{4/3}\alpha^3$	$(\frac{1-\varepsilon}{1-\varepsilon\alpha})^{2/3}\alpha^3$		

Table IV: The interfacial frictions and the coefficients according to flow regime in Tung & Dhir model

$(0 < \alpha < \alpha_1)$ Bubbly: $C_1 = 18\alpha f, C_2 = 0.34 s^3 \alpha f^2$

$$F_i = C_1 \frac{\mu_l}{D_b^2} s V_r + C_2 \frac{(s\rho_l + \alpha\rho_g)}{D_b \varepsilon} s^2 |V_r| V_r$$

$(\alpha_1 < \alpha < \alpha_2)$ Transition

$(\alpha_2 < \alpha < \alpha_3)$ Slug: $C_1 = 5.21\alpha, C_2 = 0.92 s^3 \alpha$

$$F_i = C_1 \frac{\mu_l}{D_b^2} s V_r + C_2 \frac{(s\rho_l + \alpha\rho_g)}{D_b \varepsilon} s^2 |V_r| V_r$$

$(\alpha_3 < \alpha < \alpha_4)$ Transition

$(\alpha_4 < \alpha < 1)$ Annular

$$F_i = \frac{\mu_g}{K \cdot K_{rg}} s V_r + s\alpha \frac{\rho_g}{\eta \cdot \eta_{rg}} |V_r| V_r$$

$$D_b = 1.35 \sqrt{\frac{\sigma}{g(\rho_l - \rho_g)}} \quad (7)$$

$$V_r = \frac{V_{sg}}{\alpha} - \frac{V_{sl}}{s} \quad (8)$$

$$f = \frac{1}{2}(1+\gamma)\ln(1+\frac{2}{\gamma}) \quad (9)$$

The suggested mean diameters for multi size particles are defined as Eq. 10 – 13. Where x_i is the particle size, f_i is the fraction of the number of particles in mixed bed, and the parameters (m_i , a_i , l_i and n_i) are size distribution functions by mass, area, chord length, and number of the particles, respectively.

$$d_m = \sum x_i m_i = \sum (x_i \frac{x_i^3 f_i}{\sum x_i^3 f_i}) = \frac{\sum x_i^4 f_i}{\sum x_i^3 f_i} \quad (10)$$

$$d_a = \sum x_i a_i = \sum (x_i \frac{x_i^2 f_i}{\sum x_i^2 f_i}) = \frac{\sum x_i^3 f_i}{\sum x_i^2 f_i} \quad (11)$$

$$d_l = \sum x_i l_i = \sum (x_i \frac{x_i f_i}{\sum x_i f_i}) = \frac{\sum x_i^2 f_i}{\sum x_i f_i} \quad (12)$$

$$d_n = \sum x_i n_i = \sum (x_i \frac{f_i}{\sum f_i}) \quad (13)$$

3. Experiment

3.1 PICASSO Facility

The schematic of experimental facility, called PICASSO (Pressure drop Investigation and Coolability ASSessment through Observation) is illustrated in fig. 2. It consists of filters, regulators, water and air flow meters, thermocouple, and a differential pressure transmitter. The acrylic test section with the inner diameter of 100 mm and the height of 700 mm has 6 pressure ports on the side wall. To hold particle bed and to inject air uniformly into the bed, the manufactured acrylic air distributor is placed at the bottom of the test section. It has 173 holes (ø 1.6 mm) for upward air and 108 through holes (ø 2 mm) for draining the water.

3.2 Experimental condition for the mixed bed

Table V: Properties of mixed bed

	ε	d_m [mm]	d_a [mm]	d_l [mm]	d_n [mm]
Mixed Bed	0.312	3.74	2.31	1.55	1.24

To investigate the influence of particle size distribution on pressure gradients of both single-phase air flow and water/air two-phase flow in mixed bed, and the adequacy of suggested mean diameters as the effective particle diameter, an experiment was conducted using stainless steel particles at room temperature and atmospheric pressure (20℃, 1 atm). The properties of mixed bed are listed in Table V and the particle size distribution in mixed bed is shown in fig. 1. The bed

porosity is 0.312 and various mean particle diameters for mixed bed are calculated by using Eq. 10 – 13.

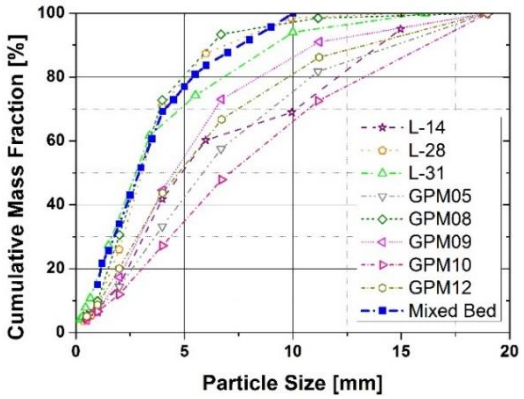

Fig. 1. Particle size distributions of previous studies [7] and mixed bed (1 – 10 mm).

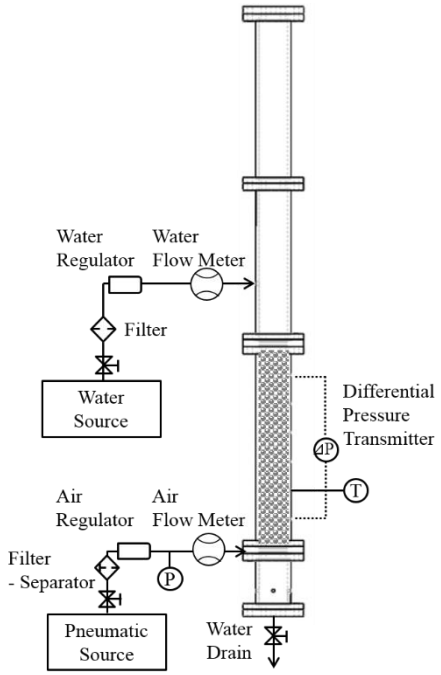

Fig. 2. Schematic of the experimental facility.

3.3 Procedure

The experimental procedure is as in the following. At the beginning of the experiment, the total mass of particles in each size is measured to obtain the bed porosity and the cumulative mass fraction, and then the particles are packed in the test section. Second, the pressure impulse lines are filled with the single-phase fluid (the air for single-phase air experiment or the water for water/air two-phase experiment). Third, the upward air is injected from the bottom of the bed, and the air flow rate and the pressure gradients are measured by data acquisition system for 5 mins when steady-state condition is established. Finally, the air flow rate is changed to another value, and immediately above step is repeated from 3 to 375 L/min.

Before the experiment, all the measurement devices were calibrated. The air flow rate was measured by one PFM7 series by SMC Korea (0.5 – 25 L/min, ±3% of full span) and two FLR 1000 series manufactured by OMEGA (20 – 100 L/min, 100 – 500 L/min) with the accuracy of ±3% of full span. And also the pressure gradients in the bed were measured by Rosemount 3051S series.

4. Experimental Results and Discussion

In fig. 3, all black filled squares are the average values of measured pressure gradients of single-phase air flow in mixed bed according to the superficial air velocity up to about 0.85 m/s and the error bars represents the maximum values between the accuracy of measurement devices and the measurement values for 5 mins in steady-state condition. Besides, the plotted lines are predicted values by the Ergun equation with various mean particle diameters. As a result of comparing the experimental data to the predictions, the experimental data is well predicted by the Ergun equation using the length mean diameter (1.55 mm) at the range of 0 – 0.7 m/s.

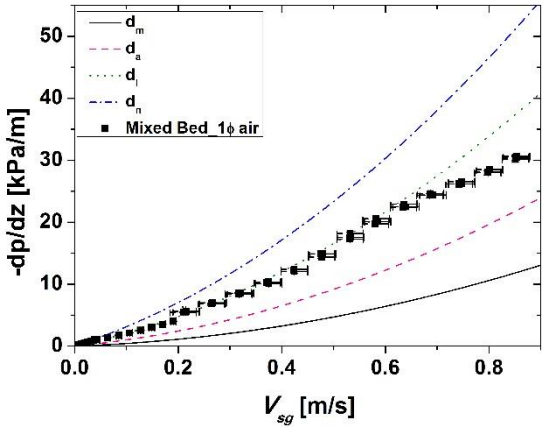

Fig. 3. Comparison of the measured pressure gradients of single-phase air flow in mixed bed to the Ergun equation using various mean diameters.

Fig. 4 shows the pressure gradients of water/air two-phase flow in mix bed with no additional water inflow. The plotted lines are predicted values by the analytical models. (i.e., Reed, R; Lipinski, L; Hu & Theofanous, HT; Schulenberg & Müller, SM; Tung & Dhir, TD). As a result of measuring the pressure gradients of water/air two-phase flow in mixed bed, it can be confirmed that there is nearly no decrease of the pressure gradients through mixed bed under superficial air velocity of 0.15 m/s. In other words, it remains at the level of hydrostatic pressure gradient which can be explained by the models without interfacial friction consideration (Reed, Lipinski and Hu & Theofanous models). On the contrary to this, those are smaller than the level of hydrostatic pressure gradient in the range of 0.15 – 0.4 m/s. It can be explained by the models considering the interfacial friction (Schulenberg & Müller and Tung & Dhir models).

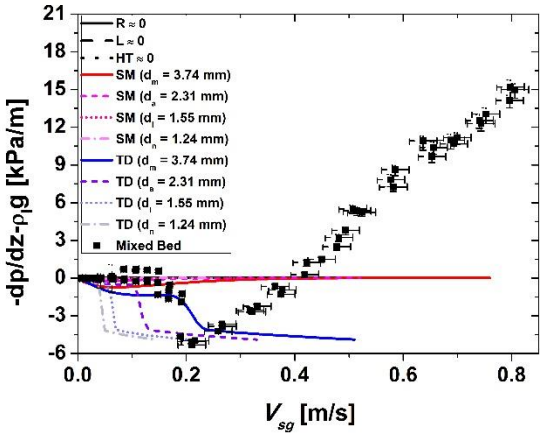

Fig. 4. Comparison of the measured pressure gradients of two-phase flow in mixed bed to analytical models.

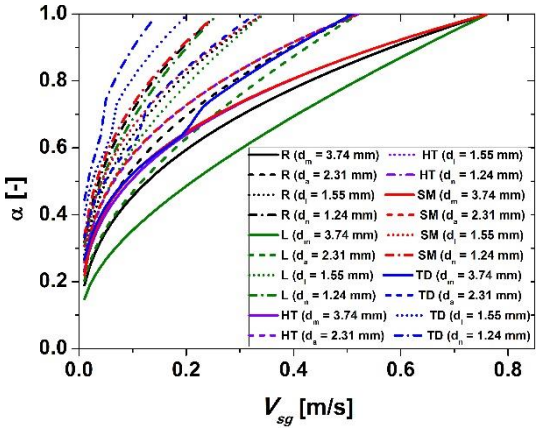

Fig. 5. Void fraction profiles resulting from analytical models adopted various mean diameters.

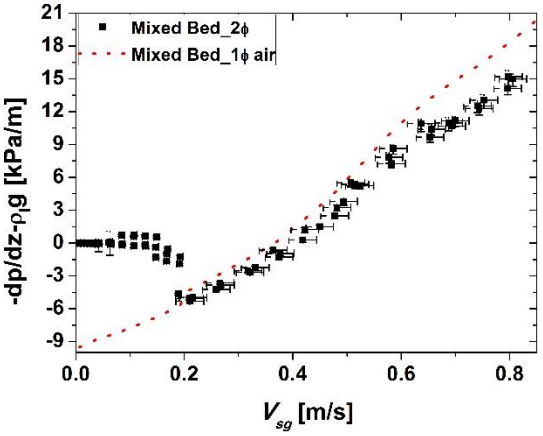

Fig. 6. Comparison of the measured pressure gradients of water/air two-phase flow to those of single-phase air flow in mixed bed.

A notable one is that the measured pressure gradients of water/air two-phase flow in mixed bed increase almost linearly at high superficial air velocity after reaching the minimum value, -5.31 kPa/m at 0.21 m/s. It is described by comparing the measured pressure gradients of two-phase flow in the mixed bed to those of single-phase air flow reduced by hydrostatic head of water column which is illustrated in fig. 6. It can be seen that the measured pressure gradients of two-phase flow in mixed bed are steeply increasing similar with those of single-phase air flow data above the superficial air velocity of 0.21 m/s. It might be explained that there exists almost upward air flow only in mixed bed though it might be considered that a small proportion of water remains at the surface of particles in mixed bed. In the comparison between experimental data and analytical models in fig. 4, it can be verified that Tung & Dhir model with the length mean diameter (1.55 mm) can predict the counter-current flow limitation at about 0.21 m/s, although it does not match well with the experimental data in the whole range of the superficial air velocity.

5. Conclusions

As a results of comparing the measured pressure gradients of single-phase air flow in mixed bed to the predicted one, the Ergun equation using the length mean diameter predicts the experimental data well at the range of 0 – 0.7 m/s. For water/air two-phase experiment, The Tung & Dhir model using the length mean diameter can predict the counter-current flow limitation although it does not predict the measured pressure gradients well for the whole range of the superficial air velocity.

6. Acknowledge

This work was supported by the Nuclear Safety Research Program through the Korea Foundation Of Nuclear Safety (KOFONS), granted financial resource from the Nuclear Safety and Security Commission (NSSC), Republic of Korea. (No. 1305008)

REFERENCES

[1] MAGALLON, D. Characteristics of corium debris bed generated in large-scale fuel-coolant interaction experiments. Nuclear Engineering and Design, 2006, 236.19: 1998-2009.
[2] LI, Liangxing; MA, Weimin. Experimental characterization of the effective particle diameter of a particulate bed packed with multi-diameter spheres. Nuclear Engineering and Design, 2011, 241.5: 1736-1745.
[3] LIPINSKI, R. J. Model for boiling and dryout in particle beds.[LMFBR]. Sandia National Labs., Albuquerque, NM (United States), 1982.
[4] HU, K.; THEOFANOUS, T. G. On the measurement and mechanism of dryout in volumetrically heated coarse particle beds. International journal of multiphase flow, 1991, 17.4: 519-532.
[5] SCHULENBERG, T.; MÜ LLER, U. An improved model for two-phase flow through beds of coarse particles. International journal of multiphase flow, 1987, 13.1: 87-97.
[6] TUNG, V. X.; DHIR, V. K. A hydrodynamic model for two-phase flow through porous media. International journal of multiphase flow, 1988, 14.1: 47-65.
[7] MORIYAMA, K, et al. Simulation of melt jet breakup and cooling in a water pool with an empirical correlation for melt particle size distribution. Proceedings of ICONE-23, 2015, 23-1672.